IEEE Access
Multidisciplinary | Rapid Review | Open Access Journal

SPECIAL SECTION ON DATA-ENABLED INTELLIGENCE FOR DIGITAL HEALTH

Received September 15, 2019, accepted October 5, 2019, date of publication October 16, 2019, date of current version October 30, 2019.

Digital Object Identifier 10.1109/ACCESS.2019.2947761

Retinal Layer Segmentation in Optical Coherence Tomography Images

BASHIR ISA DODO[1], YONGMIN LI[1], DJIBRIL KABA[2], AND XIAOHUI LIU[1]

[1]Department of Computer Science, Brunel University London, Uxbridge UB8 3PH, U.K.
[2]Connected Places Catapult, The Alan Turing Institute, London NW1 2DB, U.K.

Corresponding author: Bashir Isa Dodo (bashir.dodo@brunel.ac.uk)

ABSTRACT The four major causes of blindness are age-related diseases, out of which three affects the retina. These diseases, i.e., glaucoma, diabetic retinopathy, and age-related macular degeneration, require life-long treatment and cause irreversible blindness. Conversely, early diagnosis has been shown to curtail or prevent blindness and visual impairments. A critical element of the clinical diagnosis is the analysis of individual retinal layer properties, as the manifestation of the dominant eye diseases has been shown to correlate with structural changes to the retinal layers. Regrettably, manual segmentation is dependent on the ophthalmologist's level of expertise, and currently becoming impractical due to advancement in imaging modalities. Inherently, much research on computer-aided diagnostic methods is conducted to aid in extracting useful layer information from these images, which were inaccessible without these techniques. However, speckle noise and intensity inhomogeneity remain a challenge with a detrimental effect on the performance of automated methods. In this paper, we propose a method comprising of fuzzy image processing techniques and graph-cut methods to robustly segment optical coherence tomography (OCT) into five (5) distinct layers. Notably, the method establishes a specific region of interest to suppress the interference of speckle noise, while Fuzzy C-means is utilized to build data terms for better integration into the continuous max-flow to handle inhomogeneity. The method is evaluated on 225 OCT B-scan images, and promising experimental results were achieved. The method will allow for early diagnosis of major eye diseases by providing the basic, yet critical layer information necessary for an effective eye examination.

INDEX TERMS Medical image analysis, optical coherence tomography, fuzzy image processing, graph-cut, continuous max-flow.

I. INTRODUCTION

Prevalence of the four major causes of blindness and visual impairments, which are age-related diseases [1], calls for efficient strategies and techniques for the prevention and treatment of such diseases. A recent update by the World Health Organisation (WHO) highlights 285 million people worldwide fall victim of acute visual impairment and blindness [2], [3]. Older people from 50 years and above make up 65% of the visually impaired and 82% of the blind. Glaucoma, a disease that is known for its necessity of life long treatment, is lately estimated to account for 64.3 million people, a figure anticipated reaching 111.8 million by 2040 [4]. It is also projected that the number of victims with Age-related macular degeneration (AMD), which is the third cause of blindness, will significantly rise from 196 million in 2020 to 288 million by 2040 [5]. With such overwhelming projection estimates, there is a need for robust computer-aided diagnostic (CAD) tools, should strive to reduce this prevalence succeed.

Medical images have become an integral part of health care. Identifying features of interest such as blood vessel, optic disk, retinal layers etc. on retinal images is critical in carrying out eye screening. In particular, Optical Coherence Tomography (OCT) [6] has revolutionised the clinical eye examination as it is non-invasive imaging modality that provides high-resolution images of the retina of up to 5um. This is intrinsical because three, i.e. glaucoma, age-related macular degeneration and diabetic retinopathy, excluding cataract, out of the four major causes of eye disorder affects the retina. Although the information provided by the OCT is useful, it requires further processing to extract clinically

The associate editor coordinating the review of this manuscript and approving it for publication was Yongtao Hao.

useful information. As such, segmentation is at the core of this image-based eye examination. Currently, manual segmentation is not only tedious but also impractical due to the volume and variety of data.

Owing to the motivation and challenges mentioned above, many computer-aided diagnostic (CAD) methods have been proposed to aid in OCT analysis with varying success rates. However, these methods are restrictive. Furthermore, OCT suffers from speckle noise, which causes difficulty in the precise identification of the boundaries of layers or other structural features either through direct observation or use of segmentation algorithms [7]. The noise that corrupts OCT images is non-Gaussian, multiplicative, and neighbourhood correlated. Thus, it cannot be easily suppressed by standard software denoising methods [8]. Previous attempts, including spatial and frequency compounding techniques, have been used to address the problem of speckle-noise in OCT [9], [10]. However, these approaches can be too expensive to apply in practice, in addition to technical issues beyond discussion in our context. Additionally, digital post-processing, anisotropic diffusion filtering [11] and nonlinear anisotropic filtering [12], methods have been used for speckle noise suppression in OCT images. While these methods are effective in reducing noise, the image is either blurred or over smoothed due to loss of details (edges or lines) in non-homogeneous areas. Obviously, the purpose of pre-processing is to remove the noise without losing much detail in an image [13].

In this paper, we propose an efficient method for OCT image segmentation by utilising a combination of inexpensive methods. Distinctly, the method starts by establishing a well-defined region of interest (ROI) with all the crucial layer information. We then transform the image using fuzzy histogram hyperbolisation to improve the homogeneity within individual layers. Next, we cluster the intensity values of the transformed image into two clusters using fuzzy C-means (FCM). From the clustering outcome, a subset of pixels belonging to the hyperreflective layers is generated by thresholding the average of the subset components and their gradients by a parameter. The brightness value of these selected pixels are used to build data terms, which are integrated into an unsupervised continuous max-flow framework for computation of flow and optimisation. The method can successfully segment five (5) layers of the retina in OCT images. Specifically, the layers are identified as: Nerve Fibre Layer (NFL); Ganglion Cell + Layer-Inner Plexiform + Inner Nuclear Layer Layer(GCL+IPL+INL); Outer Plexiform Layer (OPL); Outer Nuclear Layer (ONL); Inner Segment + Outer Segment + Retinal Pigment Epithelium (IS + + OS + RPE). The locations of these layers as segmented by the method in an OCT image are illustrated in Fig. 1.

This paper is organised as follows. In Section II we revisit the literature to provide insight into current studies. Section III provides details of the proposed method, while Section IV illustrates experimental results and accompanying discussions. Lastly, Section V is reserved for concluding remarks.

II. RELATED WORKS

Image segmentation is a process of partitioning an image into non-overlapping sub-regions which are similar concerning some features such as pixel intensity or texture [14], [15]. The segmentation of retinal layers in OCT scans is not a trivial process due to the inhomogeneity, presence of vessels shadows and inherent speckle noise, variability and complexity of structures (i.e., macular, fovea and optic nerve) in pathological tissues. In recent years, several methods have been developed to detect, locate and segment different retinal layers (e.g. RNFL, GCL, IPL, etc) in OCT images [11], [16]–[28]. These segmentations methods can be grouped into three main classes based on the dimensionality of the OCT images (i.e. 1D, 2D or 3D) [29]. However, the segmentation approaches of each group differ concerning the number of retinal layer features to be extracted like intra-retinal layers or fluid-filled regions in the retinal images [29].

Early segmentation methods of OCT images are based on features extraction from either conventional pixel intensity or gradient information. However, in the literature, most of the recent segmentation methods of OCT structures are based on more complex algorithms. The most popular methods include deformable-based approaches and graph-based techniques Deformable segmentation approaches such as level sets, active contours (snakes) and geodesic active contours use the regional characteristics or edge proprieties in the image to extract tissues in the OCT images. These models are either parametric or geometric depending on the contour characteristics because they perform the segmentation using a closed curve around the target tissue and execute an iterative operation. Methods such as level-set evolve toward the OCT tissues by searching in the scan either the largest gradient or using regional features in the image. A classical deformable based retinal layers segmentation method is proposed by Yazdanpanah *et al.* [30]. The method adapts Chan-Vese's energy-minimising active contours using a multi-phase framework which incorporates a circular shape prior that model the boundaries of the retinal layers in the OCT scan and estimate the shape constraints using least squares. In [31] Wang *et al.* proposed an automated segmentation method of intra-retinal layers in a high-resolution 3D SD-OCT images. The method combines a level set algorithm, hysteresis thresholding model and multi-region continuous max-flow algorithm to extract seven intra-retinal layers including NFL, GCL+IPL, INL, OPL, ONL+IS, OS and RPE. Dodo and al, presented in [20] a level set segmentation method of seven intra-retinal layers. The method uses a region of interest and applies a gradient edges algorithm, which then use to initialise curves for the layers. The layers topology is used as a constraint in the algorithm evolution process. Although these deformable methods achieve good segmentation results, they need very robust preprocessing

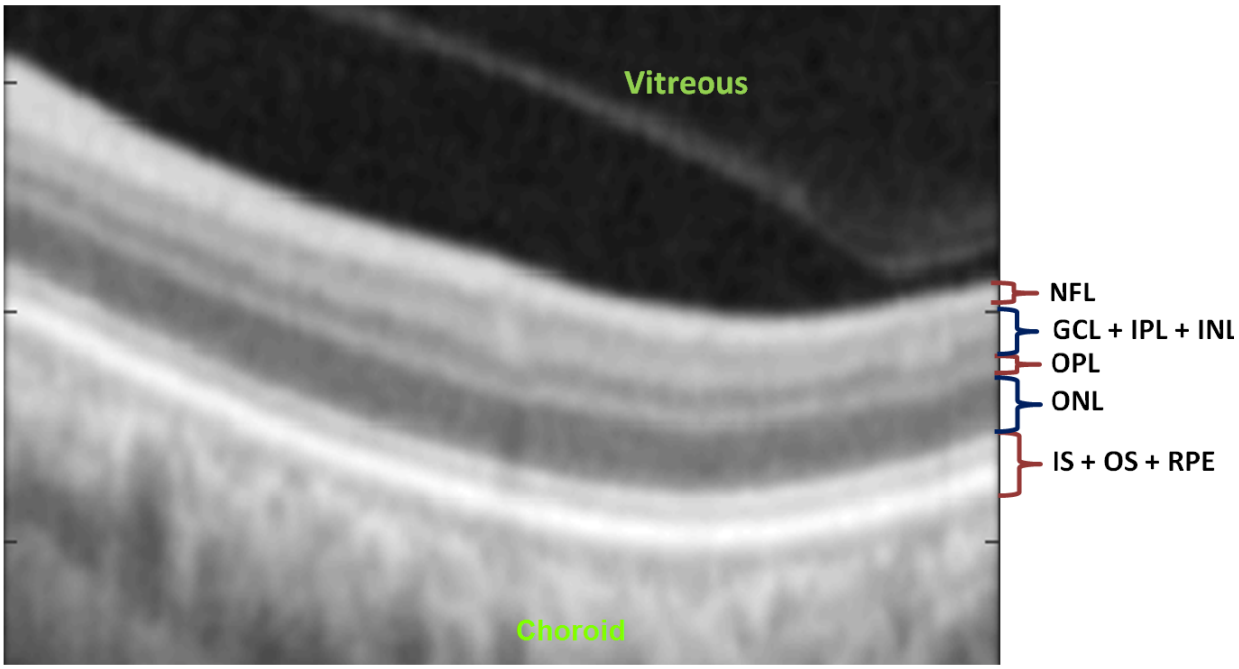

FIGURE 1. Location of the 5 retinal layers segmented in the study on an OCT image.

techniques to remove noise and imaging artefacts. They can produce poor results on heterogeneous images due to local minima. Often, the model's implementation can be complex as they use prior knowledge of the OCT image structures (i.e. pixel intensities, shapes, texture, colour, positions etc.) to define constraints on the algorithms evolution. These constraints could lead to segmentation inaccuracies when the methods are used to segment different OCT image modalities.

Like deformable segmentation approaches, graph-based methods use energy minimisation algorithms [32]–[35]. They incorporate both regional and boundary regularisation proprieties in the same manner as Mumford-Shah [36], [37]. Among all the energy optimisation approaches, graph cuts techniques are one of the most popular methods used in OCT segmentation. The methods consist of separating a graph by a maximum flow or minimum cut optimisation algorithm [38], [39], where the segmentation is performed using adjacency graph, which consists of a set of vertices (i.e. image pixels) and a set of weighted edges (i.e. weight values between two vertices) measuring the similarity between two neighbouring pixels. The segmentation is achieved by minimising a cost function which adds the values of the weights in the edges that are separated. In [17], Dodo *et al.* proposed an automated graph-cut segmentation method of retinal layers from OCT scans. This combines a fuzzy histogram hyperbolisation model and graph cut algorithm to segment eight (8) intra-retinal layers in high-resolution 3D SD-OCT images. Kaba et al. presented in [26] kernel graph cuts and continuous max-flow algorithm detect and segment the retinal layers including ILM, RNFL-GCL and RPE from circular SD-OCT scans. The segmentation is performed by adopting a multi-regional graph cut segmentation technique, that includes a kernel-induced segmentation functional and a continuous multiplier based max-flow algorithm. In [16] Antony *et al.* proposed an automated globally optimal graph-theoretic method, which simultaneously performs the segmentation of retinal layers and the micro-cystic macular edema (MME) from volumetric OCT images.

These graph-based segmentations are very applicable in the segmentation of intra-retinal layers. They can incorporate prior information such as shapes, textures, sizes, pixels seeds and position into the graph energy algorithms guiding algorithm and achieving optimal segmentation results. While the graph-based methods generate good segmentation results, their performance depends highly on both the selection of initial seed pixels and the search parameters. Another drawback is finding the right cost functions of the graph functional that can distinguish individual tissue in the OCT the scans.

Recently, with the improvement in computing power and the availability of large volume of data, various retinal layer segmentations have been explored using deep neural networks [40], [40], [40], [40], [41]. This has been very effective in medical image analysis tasks in general. A typical deep neural network for retinal layer segmentation was proposed by Fang *et al.* [40]. This segmentation method extracts nine (9) layer boundaries in OCT images of non-exudative AMD patients by combining both graph-cut search and deep neural network. In [41] He *et al.* presented a segmentation method of eight retinal layers in OCT images using a cascaded fully convolutional network (FCN) framework that guarantees the topological relationship between layers. Although deep neural networks methods achieve good

results, they rely heavily on large datasets, and they are computationally expensive to perform. They are also sensitive to biases in the datasets, which can lead to segmentation errors when used in different datasets.

We take two significant things into account in proposing this method. Firstly, by establishing a defined region of interest, the likelihood of the algorithm to find features that are not of interest is highly reduced. Secondly, the OCT is well known for its intensity inhomogeneity; as such, using fuzzy c-means (FCM) to handle the fuzzy nature of OCT is ideal. Also, using the FCM as opposed to constants in building data terms allows the method to adapt to different images. Additionally, we capitalise on domain knowledge to reduce uncertainties in both the preprocessing and segmentation steps. Specifically, we transform the images to improve homogeneity and make each layer intensity values as similar as possible using the fuzzy histogram hyperbolisation. In the segmentation stage, we improve the graph energy function by incorporating selected components belonging to the hyper-reflective layers. This improvement enables the graph cut method to differentiate the source and sink without the need for user interaction.

III. METHOD

This section details the proposed approach. A snapshot of the processes of the method is illustrated in Fig. 2. The method consists of two main parts, which are detailed in the ensuing subsections.

A. PREPROCESSING

As highlighted in the previous sections (1 and 2) and also evident in the literature, noise affects the proper identification of features of interest and negatively impacts the performance of segmentation algorithms [7], [8]. As such, we start by establishing an explicit region of interest by cropping the original image I to a cropped image $I_{cropped}$ as illustrated in Figure 3. The cropping of the image is based on domain knowledge, which is always useful in any form of analysis. Specifically for OCT image, the commonly segmented layers are within the total retinal thickness (TRT), i.e. the boundary between the retinal nerve fibre layer and the vitreous, and the boundary between the RPE and the choroid regions. Additionally, it is commonly accepted that the NFL, IS-OS and RPE exhibit high reflectivity in an OCT image [42]–[44], and based on experiments the ILM and RPE exhibits the highest transitions from dark-bright and bright-dark, respectively [17]. With these understanding of the retinal structure, we simply identify the ILM and RPE using the shortest path [45], by searching for the highest transitions on two separate adjacency matrices [42]. At this point it is fitting to crop the image I using the identified ILM and RPE points (Fig. 3 C2) and then generate a mask I_{mask} of the cropped image (Fig. 1 C3). Lastly, we multiply the mask by the original image I to retrieve the pixel intensity values within the mask, which is expressed by the equation below:

$$I_{processed} = I_{mask} * I \tag{1}$$

The result from Equation (1) is a processed image $I_{processed}$ containing part of the image with the layers information only as illustrated in Fig. 3 C4. This process of cropping on its own improves the performance of the segmentation method because with the two dominating intensity values remaining, there is less interference of image noise. It also helps in dealing with layer-like structures outside the ROI and the computational cost associated with handling image background in segmentation.

Moreover, because of the intensity inhomogeneity within individual layers and across the image, we transform the processed image using fuzzy histogram hyperbolisation [46]. This transformation is such that bright layers get higher values and the value of the dark layers becomes lower (Fig. 1 C5), which enables the segmentation of seven layers as opposed to four layers in our previous work [21]. It also further suppresses the image noise and make the intensity values within each layer as similar as possible. The preprocessing steps employed in our method is vital in our segmentation process as it enables computation of the flow strictly based on layer properties. It also allows us to utilise the full potential of the optimisation method, without having to employ complicated optimisation constraints that usually limit the method's performance.

B. SEGMENTATION

Continuous max-flow, an unsupervised segmentation method without user interaction, utilises a piece-wise constant function to model the image, where two grey values gv_1 and gv_2 are chosen to build data terms [21], [47]:

$$C_s(x) = D(f(x) - gv_1(x)), \quad C_t(x) = D(f(x) - gv_2(x)) \tag{2}$$

where $D(\cdot)$ is some penalty function. The problem with such formulation is that the distribution of values within the OCT is not equally distrubuted and fuzzy. In other words, the regions are inhomogeneous due to the incompleteness and fuzziness. Therefore, to compute the values of gv_1 and gv_2 it is convenient to employ FCM to cluster the image intensity values. This is because two main intensity values exist in the transformed image, which belong to either the bright or the dark layers. Consequently, we minimise a predefined function as follows:

$$F = \sum_x \sum_y \sum_{k=1}^{K} \mu_k^l(x,y) \, \|\zeta(x,y) - v_k\|^2 \tag{3}$$

where $\zeta(x,y)$ refers to the image intensity used as clustering trait and $\|\|$ implies Euclidean distance. We adaptively estimate the terms v_k and $\mu_k(x,y)$ denoting the estimated centroid of each cluster and the probability of each component belonging to a particular cluster, respectively, by:

$$\mu_k(x,y) = \frac{\sum_{n=1}^{K} \|\zeta(x,y) - v_n\|^{2/(l-1)}}{\|\zeta(x,y) - v_k\|^{2/(l-1)}}; \tag{4}$$

$$v_k(x,y) = \frac{\sum_x \sum_y \mu_k^l(x,y)\zeta(x,y)}{\sum_x \sum_y \mu_k^l(x,y)}. \tag{5}$$

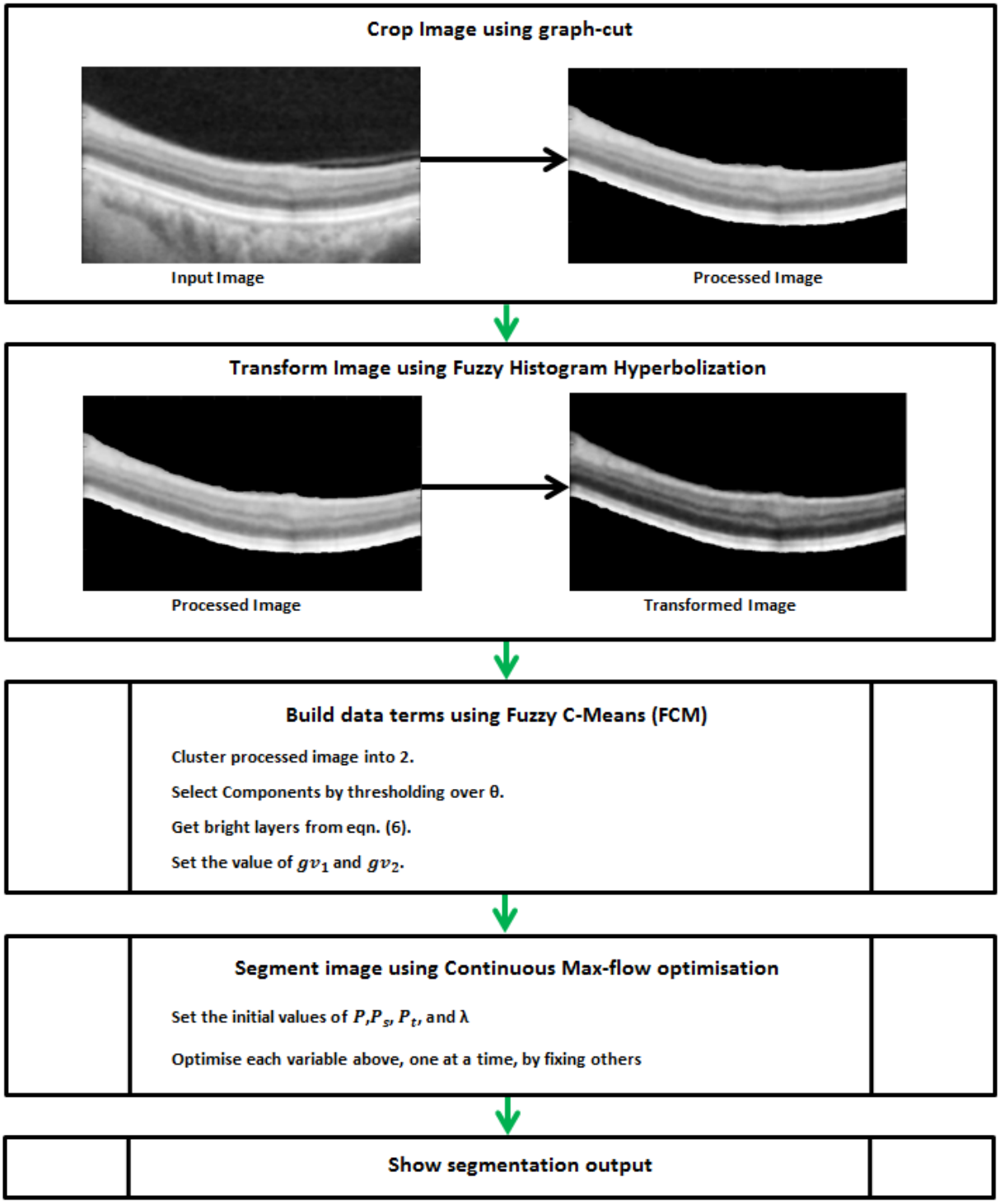

FIGURE 2. Snapshot of the proposed OCT segmentation method.

The parameter l controls the fuzziness of segmentation and its value > 1. The outcome from equation (3), $\{ \mu_k(x, y)|k = 1, 2, \ldots K \}$, is possibility of each image pixel belonging to a specific fuzzy cluster v_k. However, at this point, we are unsure of which cluster refers to the hyper-reflective layers.

Consequently, the clustering outcome μ_k is normalised and then thresholded to generate a subset containing the hyper-reflective pixels. This subsetting is to improve the probability that the components generated actually belong the hyper-reflective layers, and is computed by,

$$GV = 2\left(\sum_{1=\mu_s} Avg(\mu_s + \nabla(\mu_s)) > \theta\right) - 1. \qquad (6)$$

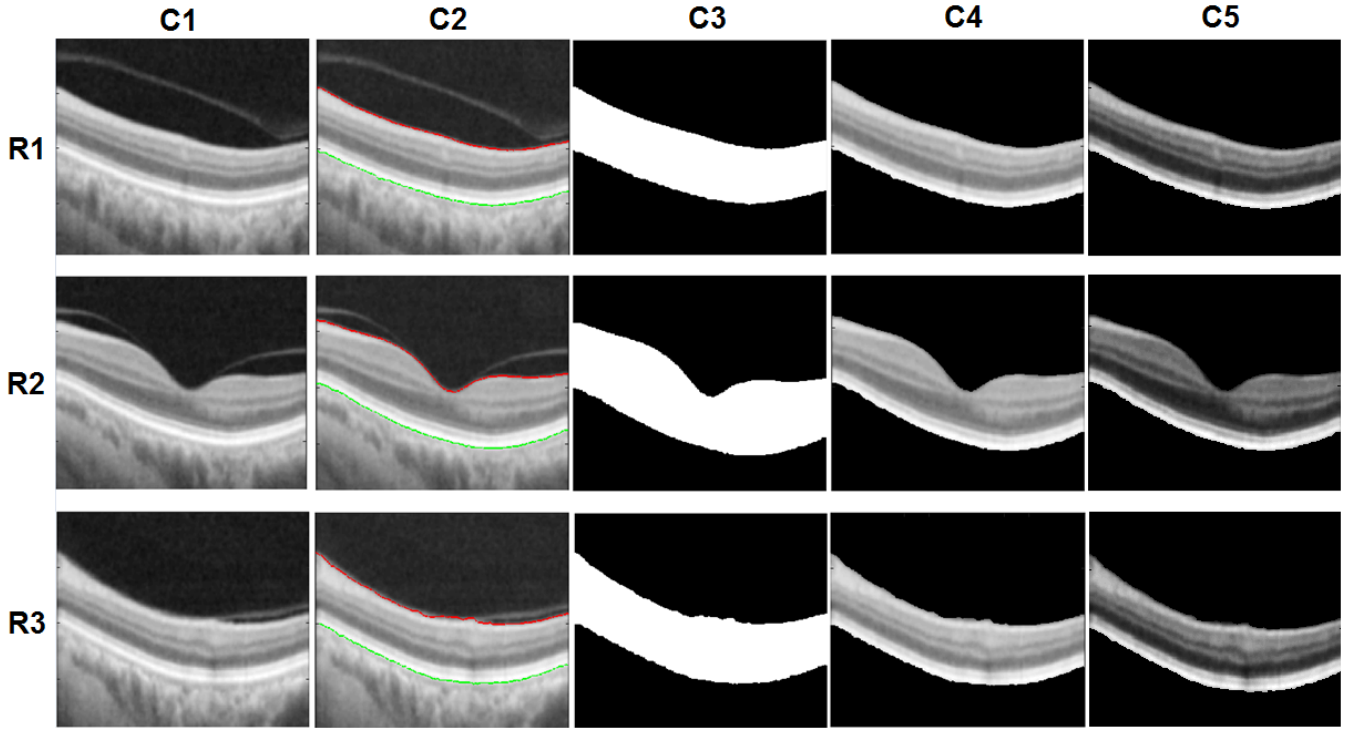

FIGURE 3. Preprocessing steps showing: R1 - Nasal region; R2 - Foveal Region; and R3- Temporal Region; C1 - Input images; C2 - identified ILM (red) and RPE (Green); C3 - image masks I_{mask}; C4 - Processed images $I_{processed}$; and C5 - Transformed images.

where μ_s refers to a subset of pixels and their normalised gradient (ranging between 0 and 1) equivalent. The parameter θ determines the components that are added to the subset and it's value ranges between 0.5 to 1. Particularly, the term μ_s is derived from

$$\mu_s = 2([\upsilon_s] > \theta) - 1, \tag{7}$$

where θ ranges between 0 and 1, and $[\upsilon_s]$ denotes a subset originating from $\mu_s = 2(\mu_k > \theta) - 1$. Specifically, $\{\ \upsilon_s | s \in S \quad \text{and} \quad S \subset K\}$.

In summary, the flow will be based on the image under examination, as opposed to the chosen priors in equation (2). We set $gv_1(x) = GV$ (i.e pixels $> \theta$ from equation (6)), while $gv_2(x)$ is determined from the pixels $< \theta$ from equation (6). Averaging the selected components and their gradient enables assertion as to which cluster components belong to the bright layers. Likewise, the value of the hypo-reflective layers will also be as close to their relative values as possible. The parameterisation of θ is important, as it allows the method to be easily adapted to the various OCT imaging modalities, which capture varying level of layer reflectivity.

By utilising the augmented Lagrangian method [48], the max-flow function can be represented as follows:

$$Lc(P_s, P_t, P, \lambda) := \int_\Omega p_s dx + \int_\Omega \lambda(divp - p_s + p_t)dx - \frac{c}{2}\|divp - p_s + p_t\|^2 \tag{8}$$

where λ is the Lagrangian multiplier introduced to optimise the flow and c is the steps in augmented Lagrangian.The spatial flow $p^*(x)$ is constrained, by imposing a condition in such a way that only saturated flows contribute to the total spatial flows and cuts, as follows:

$$C^{\alpha}_{TV} := \{p | \|p\|_\infty \leq \alpha, p_n | \partial\Omega = 0\} \tag{9}$$

where α is the penalty parameter to the total variation term $\partial\Omega$ and is constant through out. In other words, at potential cut locations x $\in \Omega$ where $\nabla\lambda^*(x) \neq 0$ the spatial flow $p^*(x)$ is saturated, while at locations x $\in \Omega$ where $|p(x)| < \alpha$ is unsaturated we must have $\nabla\lambda^*(x) = 0$ and therefore the cut does not sever the spatial domain at x. This definition enables the optimisation of the flows and the labelling of potential cuts to be executed simultaneously. The various flows and the multiplier are optimised in an iterative process until convergence.

Putting everything together from equation (8) to begin the optimisation, we initiate the values of $p_s^1 = min(C_s, C_t), p_t^1 = min(C_s, C_t), p^1 = 0, \lambda^1 = (C_s - C_t) > 0$, and then let k = 1 and start the k^{th} iteration, Optimizing p by fixing other variables

$$\begin{aligned} p^{k+1} &:= arg \max_{\|p\|\infty \leq \alpha} Lc(p_s^k, p_t^k, p, \lambda^k). \\ &= arg \max_{\|p\|\infty \leq \alpha} -\frac{c}{2}\|divp(x) - F^k\|^2 \end{aligned} \tag{10}$$

where $\prod_\alpha$ is the convex projection onto the convex set $C_\alpha = q \ |\| \ q \ \|\leq \alpha$ and F^k is a fixed variable. The above problem (10) is then computed by:

$$p^{k+1} = \prod_\alpha p^k + c\nabla(divp^k - F^k) \tag{11}$$

Optimizing p_s by fixing other variables

$$p_s^{k+1} := arg \max_{p_s(x) \leq C_s(x)} Lc(p_s, p_t^k, p^{k+1}, \lambda^k)$$
$$= arg \max_{p_s(x) \leq C_s(x)} \int_\Omega p_s dx - \frac{c}{2}\|p_s - G^k\|^2 \quad (12)$$

where G^k is a fixed variable and optimizing ps we compute at each x $\in \Omega$ pointwise;

Optimize pt by fixing other variables:

$$p_t^{k+1} := arg \max_{p_t(x) \leq C_t(x)} Lc(p_s^{k+1}, p_t, p^{k+1}, \lambda^k)$$
$$= arg \max_{p_t(x) \leq C_t(x)} -\frac{c}{2}\|p_t - H^k\|^2 \quad (13)$$

where H^k is a fixed variable and optimizing pt can be simply solved by

$$p_t(x) = \min(H^k(x), C_t(x)) \quad (14)$$

then finally update λ by:

$$\lambda^{k+1} = \lambda^k - c(divp^{k+1} \hat{a}\acute{L}' p_s^{k+1} + p_t^{k+1}) \quad (15)$$

In the event of each iteration K^{+1} the convergence criterion is determined by

$$err^k = \|\lambda^{k+}1 - \lambda^k\|/\|\lambda^{k+1}\| \quad (16)$$

The method converges if the error rate $err^* < E$ or when it reaches the maximum number of iterations. Without losing context, in-depth details regarding the augmented Lagrangian, total variation and Lipschitz principles adopted in the method are obtainable from [34], [35], [48], [49].

IV. RESULT AND DISCUSSION

The images utilised in this study were captured using the Heidelberg SD-OCT Spectralis HRA imaging system (Heidelberg Engineering, Heidelberg, Germany) in Tongren Hospital, China. Non-invasive OCT imaging centred at the macular region was performed on 13 subjects between 20 to 85 years of age. The resolution of each B-scan image is 512 pixels in depth and 992 pixels across section with 16 bits per pixel. Fifteen percent (15%) of the image height was clipped from the top to remove regions with low signal and no features of interest. Using MATLAB 2016a software, on a PC with Intel i5-4590 CPU, clock of 3.3GHz and 8GB RAM, the average computation time was 12 seconds per image.To evaluate the performance of the proposed method experiments were carried out on 225 images, 75 each from the temporal, foveal, and nasal regions. Comparing segmentation methods can be quite challenging because various studies use different data set and a variety of statistical matrices for evaluation. Also, the evaluation depends on the dimension of the data used, the standard used for comparison, e.g., labeled ground truth, the similarity between many experts, among others.

We compare the proposed method to four other methods by standardizing the number of segmented layers to five (5), which have been illustrated earlier in Fig. 1. Sample visual results of the compared methods are shown in Fig. 4. The performance of the methods is somewhat attributed to the preprocessing steps employed because it reduces the impact of image noise. Hence, the major challenge posed is in the method's ability to handle inhomogeneity. The proposed method adapts better to the inhomogeneity and inconsistency of retinal OCT images, based on experimental results to be discussed in the ensuing paragraphs.

The Root Mean Squared Error (RMSE) and Dice coefficient (DC), which are common statistical measures for evaluating the performance of segmentation algorithms, are chosen to compare the performance of the selected methods. Comparison is made between the segmentation results of the methods and the ground truth labels by computing the RMSE and DC using equation (17):

$$RMSE = \sqrt{\frac{1}{n}\sum_{i=1}^{n}(SEG_i - GT_i)^2},$$
$$DC = \frac{2 \mid GT_i \cap SEG_i \mid}{\mid GT_i \mid + \mid SEG_i \mid}, \quad (17)$$

where GT_i is the pixel labelled as part of the actual retinal layer in the manually annotated (ground truth) image and SEG_i is the pixel labelled as part of the retinal layer by the segmentation methods. n and m are the number of pixels in SEG and GT images respectively. The adaptability to the inconsistency of the retinal layers of the method is notable. This is an important factor due to the distinct retinal architecture for each person, in addition to various imaging protocols.

Furthermore, what can be deduced from Table 1 is that, the proposed method segments four (4) layers better with superior consistency as can be deduced from the values of DC and the SD in Table 1. The proposed method segments the NFL better, with RMSE and DC of **0.0179** and **0.970**, which can be attributed to the preprocessing steps in isolating the layers and the segmentation method's ability to handle intensity inconsistency. The error in Chiu *et al.* [42] is due to the inability of standard shortest path algorithms (e.g., [45]) to handle inhomogeneity such as that of the OCT. Also, [18] outperforms [20] in the NFL because in some cases the later converges at a local minimum.

Moreover, the methods in [17], [42] segmented the RPE regions better than the proposed method. Their performance is due to the region limitation, whereby the methods can search within a specific range based on the layer characteristics, and the RPE region has limited blood vessels interference. In some cases, the proposed method cuts through the OS layer due to the proximity of the layers in the region.

Consequently, the reason for the high RMSE in RPE region compared to other methods is because the proposed method has no technique of handling the proximity of the layers. Inherently, due to the regional competition in [18], it adapts to the RPE region topology better than the proposed method, although both methods do not employ region limitation or topology constraints.

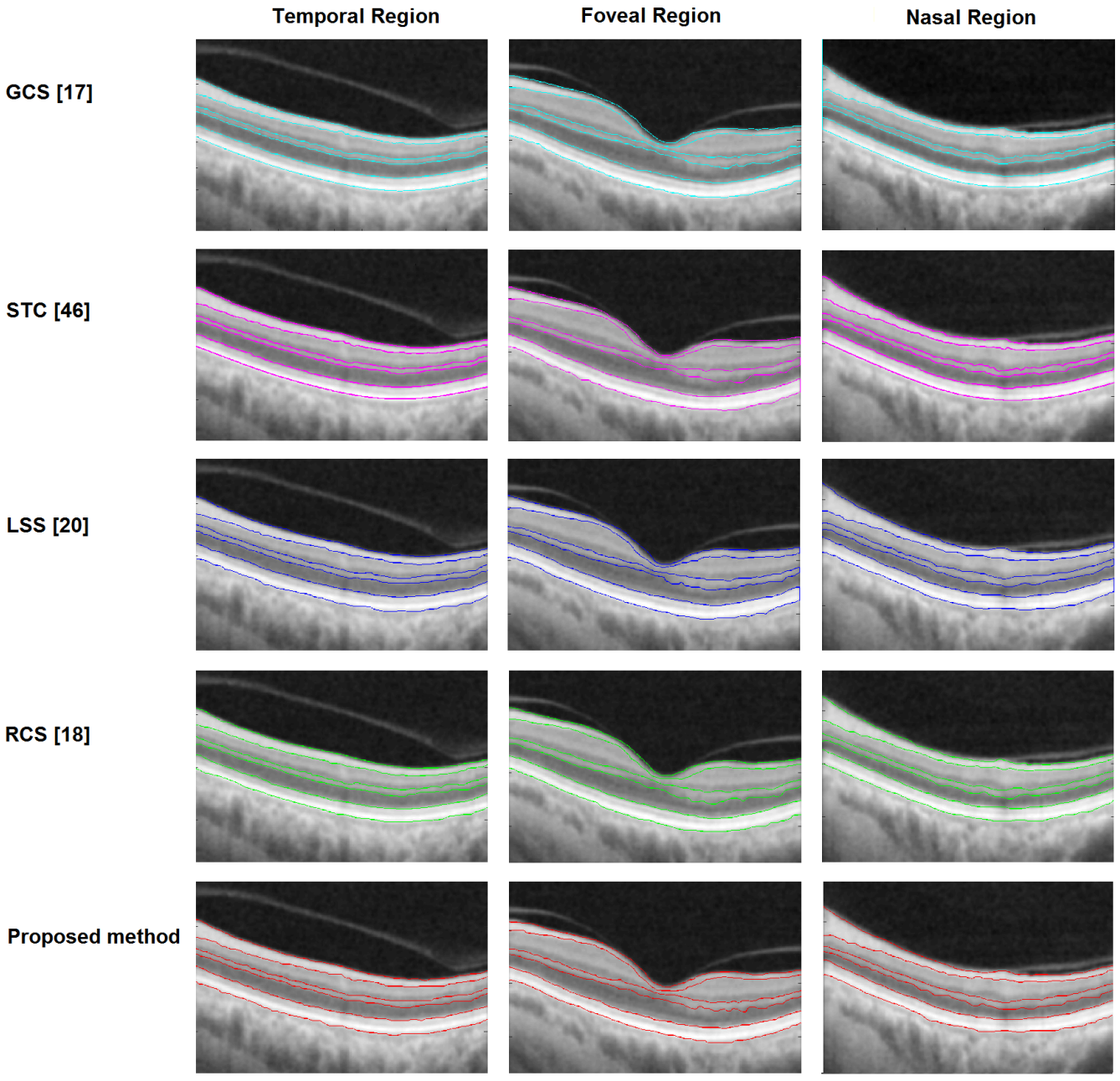

FIGURE 4. Comparison of the methods in identifying the 5 retinal layers, from left: the temporal region, center the foveal region, and right nasal region of the retina.

TABLE 1. Performance evaluation on 225 OCT images showing values of the Root Mean Squared Error (RMSE) and Dice Coefficient (DC) (and standard deviation (SD)) in comparison to the true layer labeling (units in pixels).

Layer Name	NFL		GCL - INL		OPL		ONL		IS - RPE	
Method	RMSE	DC (SD)	RMSE	DC (SD)	RMSE	DC (SD)	RMSE	DC (SD)	RMSE	DC (SD)
GCS [17]	0.0198	0.964 (0.026)	0.381	0.881 (0.036)	0.0380	0.836 (0.039)	0.0365	0.878 (0.045)	**0.0232**	**0.939 (0.021)**
STC [42]	0.0312	0.919 (0.083)	0.0442	0.879 (0.043)	0.0466	0.802 (0.040)	0.0381	0.856 (0.051)	0.0249	0.934 (0.024)
LSS [20]	0.0286	0.921 (0.026)	0.390	0.883 (0.061)	0.0418	0.852 (0.042)	0.0379	0.884 (0.053)	0.0331	0.918 (0.027)
RCS [18]	0.0273	0.933 (0.031)	0.0429	0.875 (0.038)	0.0402	0.867 (0.036)	0.0348	0.879 (0.049)	0.0319	0.923 (0.020)
Proposed method	**0.0179**	**0.970 (0.029)**	**0.0293**	**0.890 (0.037)**	**0.0274**	**0.894 (0.048)**	**0.0283**	**0.895 (0.039)**	0.0255	0.926 (0.023)

Generally, region limitation based on retinal layer topology aids in handling incompleteness in [17], [20], [42], while FCM aids in handling inhomogeneity within layers by adaptively estimating values specific to each image in [18] and the proposed method. This can be deduced from the NFL layer performance discussed earlier based on the performance matrix in Table 1, and in comparison of [18] and the proposed method to [17], [42] for the level set and graph cut methods,

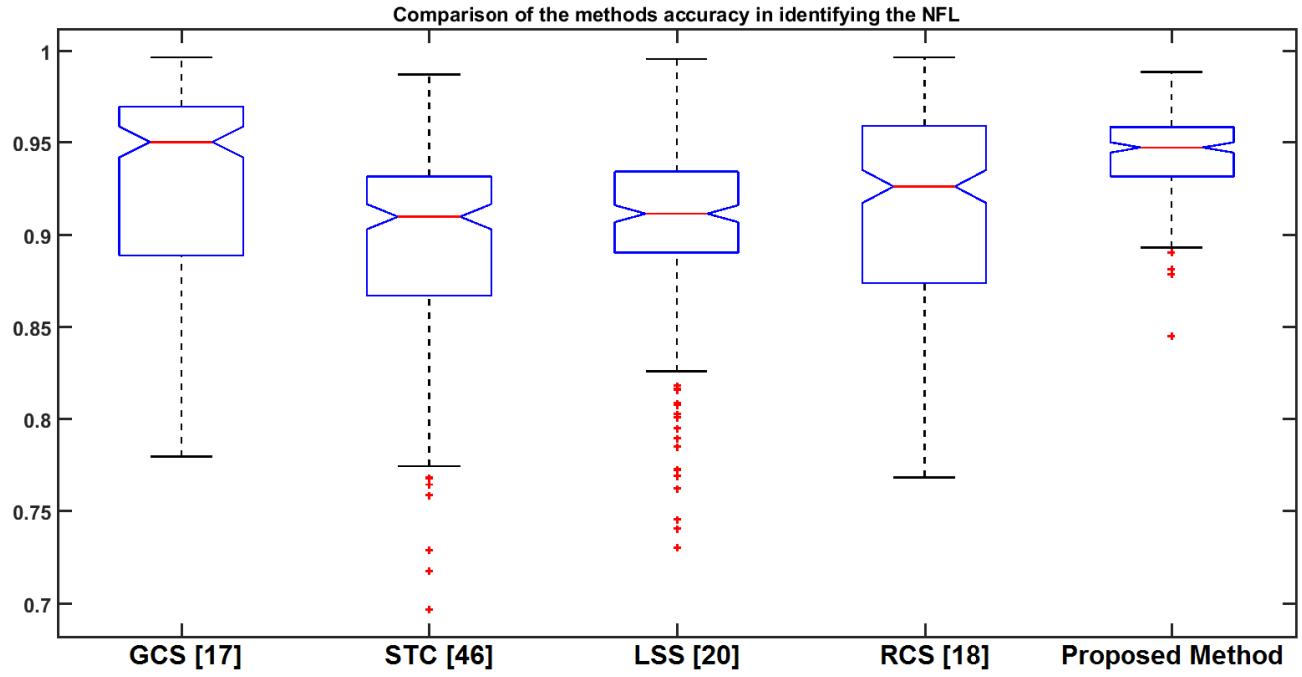

FIGURE 5. Boxplot of the distribution of accuracy in segmenting retinal nerve fibre layer thickness results from Table 2.

respectively. Also, the reinforced FCM influence is portrayed in the GCL to IPL, OPL, and ONL regions, except for the fact that the proposed method segments these layers better than [18]. This is mainly because the transformation of the image makes the layers unique, making it more convenient for continuous max-flow to identify the layers.

Due to the importance of the retinal nerve fibre layer in diagnosing eye diseases (and recently neurological and other terminal diseases), it is further assessed with the accuracy measure computer by:

$$Accuracy = \frac{TP + TN}{(TP + FP + FN + TN)} \tag{18}$$

where the terms TP, TN, FP and FN refers to true positive, true negative, false positive and false negative respectively. Distinctly, TP represents the number of pixels which are part of the region in the ground truth that is labelled correctly by the segmentation methods. TN represents the number of pixels which are part of the background region in the ground truth and labelled correctly by the methods. FP denotes the pixels labelled as a part of the region by the methods but are actually part of the background in the ground truth. Lastly, the term FN represents the pixels labelled as a part of the background by the methods but are truly part of the region in the ground truth. The performance of the methods using the accuracy criteria (equation (18)) is shown in Table 2 while the distribution of the values is shown in Fig. 5. The method proposed herein achieved a good result and is consistent. The distribution of the accuracy in the box plot shows high accuracy and efficiency of the method.

What we can deduce from Table 2 is that the proposed method achieves high accuracy of $\sim$ 95%, with

TABLE 2. Performance evaluation on 225 OCT images showing values of accuracy (standard deviation (SD)) of the methods in identifying the Nerve Fibre Layer (NFL)(units in pixels).

Method	Accuracy Mean (SD)
GCS [17]	0.9281 (0.053)
STC [42]	0.8977 (0.058)
LSS [20]	0.9045 (0.050)
RCS [18]	0.9144 (0.052)
Proposed method	**0.9440 (0.022)**

accompanying consistency and adaptability to the contour variance of the OCT, which is further affirmed by the distribution of values in Fig. 5. Although the methods in [17], [18] have no outliers beyond the first quartile, their accuracy values start from $\sim$ 76% which is low compared to the starting value of $\sim$ 84% of the proposed method. The method in [20] has the second-best start of the first quartile. However, it has underperformed in identifying the NFL in few images due to the constraints set by the method (+ from Fig. 5).

In theory, the proposed method outperforms the other methods because the bright layers have been isolated and the max-flow min-cut algorithm is able to locate the points where the change is greatest, and there is the minimum relationship between the nodes. The graph cut methods outperform the level set methods. Although the methods in [18] and [20] have improved performance than classic level set methods, they evolve based on forces to a defined optimum.

Generally, the graph-cut methods [17], [42] outperformed the level set methods [18], [20] in OCT image segmentation, which was not the expectation at the beginning of the experiments. While the level set method was able to segment more layers than the graph-based methods. It is to be noted that these observations are limited to the scope of this research,

which can provide an avenue for further exploration. In particular, the proposed method performs better because it optimises the flow and then finds the layer boundaries. It is as if the max-flow min-cut algorithm is innate for segmentation problems, where the goal is to find the greatest change from the standard layer distribution, which also refers to the point where the layers differ the most. The full potential of the technology in retinal image analysis is yet to be fully utilised as commercial systems focus on segmenting only a few layers of the retina. Eye diseases pose a threat to the quality of life, which makes it critical to prevent them with new technology by leveraging the knowledge available.

V. CONCLUSION

This study presents a fully automatic and simultaneous method to segment five (5) layers from an OCT image by utilizing domain knowledge and inexpensive computational methods. The main contributions of this work can be summarised as follows.

First, fuzzy histogram hyperbolisation is employed to transform the distinct ROI to improve the homogeneity within individual layers without distorting image information. As opposed to filtering and averaging denoising methods, which usually require a filter window or threshold, we utilize domain knowledge to preprocess the image to reduce the effect of noise and improve homogeneity. Specifically, the cropping of the image to contain the layers only promotes accurate segmentation, while the improved fuzzy histogram hyperbolisation transformation improves segmentation results by reducing image noise and inhomogeneity. The preprocessing steps we employ in our approach can be easily adapted to improve the performance of segmentation methods, based on the fact that the steps improve similarity and difference within the image, which forms the basis of image segmentation.

Second, the desirable data terms are computed by selecting the unique hyperreflective layers of the retina, which then are integrated into the continuous max-flow graph-cut framework for robust segmentation. The continuous max-flow can handle intensity inconsistency within the image by building data terms (gv_1 and gv_2) unique for each image with the aid of the reinforced Fuzzy C-Means. This approach is ideal for OCT segmentation, because the intensity values of OCT vary even within each layer, depending on image noise and imaging modality. Also, the successful assignment of appropriate weight based on unique image features contributes to the plausible performance of our method, taking into account graph-cut methods depends on the assignment of appropriate weights.

The method plausibly segments 5 layers.The number of layers can be improved by adjusting the value of T and P, such that pixels from other regions not segmented in this study can be included in the distinct ROI. However this requires further techniques to handle the incompleteness of the layers, which the refinement of the edges and extrapolation can contribute to achieving such.

REFERENCES

[1] R. Klein and B. E. K. Klein, "The prevalence of age-related eye diseases and visual impairment in aging: Current estimates," *Investigative Ophthalmol. Vis. Sci.*, vol. 54, no. 14, pp. ORSF5–ORSF13, 2013.

[2] M. Zetterberg, "Age-related eye disease and gender," *Maturitas*, vol. 83, pp. 19–26, Jan. 2016.

[3] *Global Data on Visual Impairments 2010*, document WHO/NMH/PBD/12.01, Geneva, Switzerland, 2012. [Online]. Available: http://www.who.int/about/regions/en/index.html

[4] Y.-C. Tham, X. Li, T. Y. Wong, H. A. Quigley, T. Aung, and C.-Y. Cheng, "Global prevalence of glaucoma and projections of glaucoma burden through 2040: A systematic review and meta-analysis," *Ophthalmology*, vol. 121, no. 11, pp. 2081–2090, 2014.

[5] A. P. Yow, D. Wong, H. Liu, H. Zhu, I. J.-W. Ong, A. Laude, and T. H. Lim, "Automatic visual impairment detection system for age-related eye diseases through gaze analysis," in *Proc. 39th Annu. Int. Conf. IEEE Eng. Med. Biol. Soc. (EMBC)*, Jul. 2017, pp. 2450–2453.

[6] D. Huang, E. A. Swanson, C. P. Lin, J. S. Schuman, W. G. Stinson, W. Chang, M. R. Hee, T. Flotte, K. Gregory, and C. A. Puliafito, "Optical coherence tomography.," *Science*, vol. 254, no. 5035, pp. 1178–1181, 1991.

[7] A. Mishra, A. Wong, K. Bizheva, and D. A. Clausi, "Intra-retinal layer segmentation in optical coherence tomography images," *Opt. Express*, vol. 17, no. 26, pp. 23719–23728, 2009.

[8] M. A. Mayer, J. Hornegger, C. Y. Mardin, and R. P. Tornow, "Retinal nerve fiber layer segmentation on FD-OCT scans of normal subjects and glaucoma patients," *Biomed. Opt. Express*, vol. 1, no. 5, pp. 1358–1383, 2010.

[9] N. Iftimia, B. E. Bouma, and G. J. Tearney, "Speckle reduction in optical coherence tomography by 'path length encoded' angular compounding," *J. Biomed. Opt.*, vol. 8, no. 2, pp. 260–263, 2003.

[10] M. Pircher, E. Götzinger, R. Leitgeb, A. F. Fercher, and C. K. Hitzenberger, "Speckle reduction in optical coherence tomography by frequency compounding," *J. Biomed. Opt.*, vol. 8, no. 3, pp. 565–569, Jul. 2003.

[11] D. C. Fernandez, "Delineating fluid-filled region boundaries in optical coherence tomography images of the retina," *IEEE Trans. Med. Imag.*, vol. 24, no. 8, pp. 939–945, Aug. 2005.

[12] G. Gregori and R. W. Knighton, "A robust algorithm for retinal thickness measurements using optical coherence tomography (stratus OCT)," *Investigative Ophthalmol. Vis. Sci.*, vol. 45, no. 13, p. 3007, May 2004.

[13] H. M. Salinas and D. C. Fernandez, "Comparison of PDE-based nonlinear diffusion approaches for image enhancement and denoising in optical coherence tomography," *IEEE Trans. Med. Imag.*, vol. 26, no. 6, pp. 761–771, Jun. 2007.

[14] N. R. Pal and S. K. Pal, "A review on image segmentation techniques," *Pattern Recognit.*, vol. 26, no. 9, pp. 1277–1294, 1993.

[15] N. M. Zaitoun and M. J. Aqel, "Survey on image segmentation techniques," *Procedia Comput. Sci.*, vol. 65, pp. 797–806, Jan. 2015.

[16] B. J. Antony, A. Lang, E. K. Swingle, O. Al-Louzi, A. Carass, S. Solomon, P. A. Calabresi, S. Saidha, and J. L. Prince, "Simultaneous segmentation of retinal surfaces and microcystic macular edema in SDOCT volumes," in *Medical Imaging 2016: Image Processing*. 2016.

[17] B. I. Dodo, Y. Li, K. Eltayef, and X. Liu, "Graph-cut segmentation of retinal layers from OCT images," in *Proc. 11th Int. Joint Conf. Biomed. Eng. Syst. Technol. (BIOIMAGING)*, vol. 2, 2018, pp. 35–42.

[18] B. I. Dodo, Y. Li, A. Tucker, D. Kaba, and X. Liu, "Retinal OCT segmentation using fuzzy region competition and level set methods," in *Proc. IEEE 32nd Int. Symp. Comput.-Based Med. Syst. (CBMS)*, Jun. 2019, pp. 93–98.

[19] C. Wang, Y. Wang, D. Kaba, Z. Wang, X. Liu, and Y. Li, "Automated layer segmentation of 3D macular images using hybrid methods," in *Proc. Int. Conf. Image Graph.*, Tianjing, China, vol. 9217, 2015, pp. 614–628.

[20] B. I. Dodo, Y. Li, X. Liu, and M. I. Dodo, "Level set segmentation of retinal OCT images," in *Proc. 12th Int. Joint Conf. Biomed. Eng. Syst. Technol.*, vol. 2, 2019, pp. 49–56.

[21] B. I. Dodo, Y. Li, and X. Liu, "Retinal OCT image segmentation using fuzzy histogram hyperbolization and continuous max-flow," in *Proc. IEEE 30th Int. Symp. Comput.-Based Med. Syst. (CBMS)*, Jun. 2017, pp. 745–750.

[22] G. Quellec, K. Lee, M. Dolejsi, M. K. Garvin, M. D. Abramoff, and M. Sonka, "Three-dimensional analysis of retinal layer texture: Identification of fluid-filled regions in SD-OCT of the macula," *IEEE Trans. Med. Imag.*, vol. 29, no. 6, pp. 1321–1330, Jun. 2010.

[23] F. Rathke, S. Schmidt, and C. Schnörr, "Probabilistic intra-retinal layer segmentation in 3-D OCT images using global shape regularization," *Med. Image Anal.*, vol. 18, no. 5, pp. 781–794, 2014.
[24] M. K. Garvin, M. D. Abramoff, R. Kardon, S. R. Russell, X. Wu, and M. Sonka, "Intraretinal layer segmentation of macular optical coherence tomography images using optimal 3-D graph search," *IEEE Trans. Med. Imag.*, vol. 27, no. 10, pp. 1495–1505, Oct. 2008.
[25] A. Yazdanpanah, G. Hamarneh, B. R. Smith, and M. V. Sarunic, "Segmentation of intra-retinal layers from optical coherence tomography images using an active contour approach," *IEEE Trans. Med. Imag.*, vol. 30, no. 2, pp. 484–496, Feb. 2011.
[26] D. Kaba, Y. Wang, C. Wang, X. Liu, H. Zhu, A. G. Salazar-Gonzalez, and Y. Li, "Retina layer segmentation using kernel graph cuts and continuous max-flow," *Opt. Express*, vol. 23, no. 6, pp. 7366–7384, 2015.
[27] K. Lee, M. Niemeijer, M. K. Garvin, Y. H. Kwon, M. Sonka, and M. D. Abramoff, "Segmentation of the optic disc in 3-D OCT scans of the optic nerve head," *IEEE Trans. Med. Imag.*, vol. 29, no. 1, pp. 68–159, Jan. 2010.
[28] B. J. Antony, M. D. Abràmoff, M. Sonka, Y. H. Kwon, and M. K. Garvin, "Incorporation of texture-based features in optimal graph-theoretic approach with application to the 3D segmentation of intraretinal surfaces in SD-OCT volumes," *Proc. SPIE*, vol. 8314, Feb. 2012, Art. no. 83141G.
[29] D. Cabrera, "A review of algorithms for segmentation of retinal image data using optical coherence tomography," in *Image Segmentation*. 2012.
[30] A. Yazdanpanah, G. Hamarneh, B. Smith, and M. Sarunic, "Intraretinal layer segmentation in optical coherence tomography using an active contour approach," in *Proc. Int. Conf. Med. Image Comput. Comput.-Assist. Intervent.* Springer, 2009, pp. 649–656.
[31] Z. Wang, M. W. Jenkins, G. C. Linderman, H. G. Bezerra, Y. Fujino, M. A. Costa, D. L. Wilson, and A. M. Rollins, "3-D stent detection in intravascular OCT using a Bayesian network and graph search," *IEEE Trans. Med. Imag.*, vol. 34, no. 7, pp. 1549–1561, Jul. 2015.
[32] Y. Boykov and G. Funka-Lea, "Graph cuts and efficient N-D image segmentation," *Int. J. Comput. Vis.*, vol. 70, no. 2, pp. 109–131, Nov. 2006.
[33] Y. Y. Boykov and M.-P. Jolly, "Interactive graph cuts for optimal boundary & region segmentation of objects in N-D images," in *Proc. 8th IEEE Int. Conf. Comput. Vis. (ICCV)*, vol. 1, Jul. 2001, pp. 105–112.
[34] V. Kolmogorov and R. Zabin, "What energy functions can be minimized via graph cuts?" *IEEE Trans. Pattern Anal. Mach. Intell.*, vol. 26, no. 2, pp. 147–159, Feb. 2004.
[35] Y. Boykov, O. Veksler, and R. Zabih, "Fast approximate energy minimization via graph cuts," *IEEE Trans. Pattern Anal. Mach. Intell.*, vol. 23, no. 11, pp. 1222–1239, Nov. 2001.
[36] J. Petitot, "An introduction to the Mumford–Shah segmentation model," *J. Physiol.-Paris*, vol. 97, pp. 335–342, Mar./May 2003.
[37] B. Bourdin and A. Chambolle, "Implementation of an adaptive finite-element approximation of the Mumford-Shah functional," *Numerische Mathematik*, vol. 85, no. 4, pp. 609–646, 2000.
[38] D. M. Greig, B. T. Porteous, and A. H. Seheult, "Exact maximum *A Posteriori* estimation for binary images," *J. Roy. Stat. Soc.*, vol. 51, no. 2, pp. 271–279, 1989.
[39] L. R. Ford, Jr., and D. R. Fulkerson, "Maximal flow through a network," *Canad. J. Math.*, vol. 8, no. 3, pp. 399–404, 1956.
[40] L. Fang, D. Cunefare, C. Wang, R. H. Guymer, S. Li, and S. Farsiu, "Automatic segmentation of nine retinal layer boundaries in OCT images of non-exudative AMD patients using deep learning and graph search," *Biomed. Opt. Express*, vol. 8, no. 5, pp. 2732–2744, 2017.
[41] Y. He, A. Carass, Y. Yun, C. Zhao, B. M. Jedynak, S. D. Solomon, S. Saidh0a, P. A. Calabresi, and J. L. Prince, "Towards topological correct segmentation of macular OCT from cascaded FCNs," in *Fetal, Infant and Ophthalmic Medical Image Analysis*. Springer, 2017, pp. 202–209.
[42] S. J. Chiu, X. T. Li, P. Nicholas, C. A. Toth, J. A. Izatt, and S. Farsiu, "Automatic segmentation of seven retinal layers in SDOCT images congruent with expert manual segmentation," *Opt. Express*, vol. 18, no. 18, pp. 19413–19428, 2010.
[43] Q. Dai and Y. Sun, "Automated layer segmentation of optical coherence tomography images," in *Proc. 4th Int. Conf. Biomed. Eng. Inform. (BMEI)*, Oct. 2011, vol. 1, no. 10, pp. 142–146.
[44] J. Tian, B. Varga, G. M. Somfai, W.-H. Lee, W. E. Smiddy, and D. C. DeBuc, "Real-time automatic segmentation of optical coherence tomography volume data of the macular region," *PLoS One*, vol. 10, no. 8, 2015, Art. no. e0133908.
[45] E. W. Dijkstra, "A note on two problems in connexion with graphs," *Numer. Math.*, vol. 1, no. 1, pp. 269–271, Dec. 1959.
[46] H. R. Tizhoosh and M. Fochem, "Fuzzy histogram hyperbolization for image enhancement," *Proc. EUFIT*, vol. 95, pp. 1695–1698, Jan. 1995.
[47] J. Yuan, E. Bae, and X.-C. Tai, "A study on continuous max-flow and min-cut approaches," in *Proc. IEEE Conf. Soc. Conf. Comput. Vis. Pattern Recognit.*, vol. 7, Jun. 2010, pp. 2217–2224.
[48] D. P. Bertsekas, *Nonlinear Programming*. Belmont, MA, USA: Athena Scientific, 1999.
[49] Y. Boykov and V. Kolmogorov, "An experimental comparison of min-cut/max- flow algorithms for energy minimization in vision," *IEEE Trans. Pattern Anal. Mach. Intell.*, vol. 26, no. 9, pp. 1124–1137, Sep. 2004.

BASHIR ISA DODO received the B.Sc. degree (Hons.) in software engineering and the M.Sc. degree in computer systems engineering (software systems) from the University of East London, U.K., in 2011 and 2013, respectively. He is currently pursuing the Ph.D. degree with the Department of Computer Science, Brunel University London, U.K. He was an Assistant Lecturer with Umaru Musa Yar'adua University, Nigeria, from 2013 to 2015. His research interests include software engineering, motion detection, computer vision, image processing, medical image analysis, and big data analytics.

YONGMIN LI received the B.Eng. and M.Eng. degrees in control engineering from Tsinghua University, Beijing, China, in 1990 and 1992, respectively, and the Ph.D. degree in computer vision from the Queen Mary University of London, U.K., in 2001. From 2001 to 2003, he was a Research Scientist with British Telecom Laboratories, Suffolk, U.K. He is currently a Senior Lecturer with the Department of Computer Science, Brunel University London, U.K. His current research interests include automatic control, nonlinear filtering, computer vision, image processing, video analysis, medical imaging, machine learning, and pattern recognition.

DJIBRIL KABA received the B.Eng. and M.Eng. degrees in electronics engineering from King's College London, London, U.K., in 2010, and the Ph.D. degree in computer science from Brunel University London, West London, U.K., in 2013. His research interests include machine learning, artificial intelligent, deep learning, computer vision, pattern recognition, and medical images analysis.

XIAOHUI LIU received the B.Eng. degree in computing from Hohai University, Nanjing, China, in 1982, and the Ph.D. degree in computer science from Heriot-Watt University, Edinburgh, U.K., in 1988. He is currently a Professor of computing with Brunel University London, West London, U.K., where he directs the Centre for Intelligent Data Analysis, conducting interdisciplinary research concerned with the effective analysis of data. He is also a Professor of computing with King Abdulaziz University, Jeddah, Saudi Arabia. He has over 100 high-quality journal publications in biomedical informatics, complex systems, computational intelligence, and data mining. He is a Charted Engineer, a Life Member of the Association for the Advancement of Artificial Intelligence, a Fellow of the Royal Statistical Society, and a Fellow of the British Computer Society. His H-index is over 40.